ADVANCED HEALTHCARE MATERIALS
www.advhealthmat.de

Integrated Cascade Nanozyme Remodels Chondrocyte Inflammatory Microenvironment in Temporomandibular Joint Osteoarthritis via Inhibiting ROS-NF-κB and MAPK Pathways

Zhongyin Zhang, Lichan Yuan, Yufeng Liu, Ruobing Wang, Yihong Zhang, Yan Yang, Hui Wei, and Junqing Ma**

Temporomandibular joint osteoarthritis (TMJ OA) is a degenerative joint disease with no complete cure at present. Notably, the inflammatory microenvironment in TMJ OA is modulated by oxidative stress, which impacts cartilage metabolism, chondrocyte apoptosis, inflammatory cytokine release, and extracellular matrix (ECM) synthesis. Thus, it is reasoned that reducing excess reactive oxygen species (ROS) in the chondrocyte microenvironment may be an effective therapeutic strategy for TMJ OA. Recently, cascade nanozymes, including Pt@PCN222-Mn, have been exploited to treat ROS-associated diseases. Nevertheless, cascade nanozymes are not employed for TMJ OA therapy. To fill this gap, it is explored whether the Pt@PCN222-Mn cascade nanozyme could be applied to the treatment of TMJ OA. The in vitro results demonstrate that the Pt@PCN222-Mn nanozyme can inhibit the production of inflammatory factors, the degradation of ECM, and the apoptosis of chondrocytes by inhibiting the ROS-nuclear factor kappa-B (NF-κB_ and mitogen-activated protein kinase signaling pathways. The in vivo results further demonstrate that the Pt@PCN222-Mn nanozyme can delay the progression of TMJ OA in the rat unilateral anterior crossbite model. It is believed that insightful perspectives on the application of nanozymes in TMJ OA will be provided here.

1. Introduction

Temporomandibular disorder (TMD) is a heterogeneous masticatory system disorder that occurs mostly in young female adults. Temporomandibular joint osteoarthritis (TMJ OA) is a severe subtype of TMD.[1] TMJ OA is a kind of degenerative joint disease characterized by chondrocyte apoptosis and inflammation, extracellular matrix (ECM) degradation, and abnormal remodeling of subchondral bone.[2] In the clinic, conservative therapies are preferable for patients in the early or intermediate stages, including medication, occlusal splints, intra-articular (IA) injections, and arthroscopy.[3] However, systemic side effects associated with oral medications, such as gastrointestinal damage, cardiovascular risk, and frequent IA injections, may lead to dizziness, dry mouth, and even addiction.[4] Furthermore, open joint surgery is only performed in severe cases that are associated with high complications.[5] Although new IA system therapies such as tissue engineering, immunology, and gene therapy have come to light in recent years,[6] these therapies have only been tested in a few studies, which means that innovative treatments for TMJ OA remain unmet clinically. Reactive oxygen species (ROS) plays a crucial role as a new second messenger in the physiological and pathological processes of the body. Meanwhile, oxidative stress is closely associated with the destabilization of the TMJ OA microenvironment.[3,7] Growing evidence reveals that ROS

Z. Zhang, L. Yuan, R. Wang, Y. Yang, J. Ma
Jiangsu Key Laboratory of Oral Diseases
Nanjing Medical University
140 Hanzhong Road, Nanjing, Jiangsu 210029, China
E-mail: jma@njmu.edu.cn
Z. Zhang, L. Yuan, R. Wang, Y. Yang, J. Ma
Department of Orthodontics
The Affiliated Stomatological Hospital of Nanjing Medical University
136 Hanzhong Road, Nanjing, Jiangsu 210029, China

The ORCID identification number(s) for the author(s) of this article can be found under https://doi.org/10.1002/adhm.202203195

DOI: 10.1002/adhm.202203195

Y. Liu, Y. Zhang, H. Wei
Department of Biomedical Engineering
College of Engineering and Applied Sciences
Nanjing National Laboratory of Microstructures
Jiangsu Key Laboratory of Artificial Functional Materials
Chemistry and Biomedicine Innovation Center (ChemBIC)
Nanjing University
Nanjing, Jiangsu 210023, China
E-mail: weihui@nju.edu.cn
Y. Liu
Jiangsu Key Laboratory of New Drug Research and Clinical Pharmacy
Xuzhou Medical University
Xuzhou, Jiangsu 221002, China

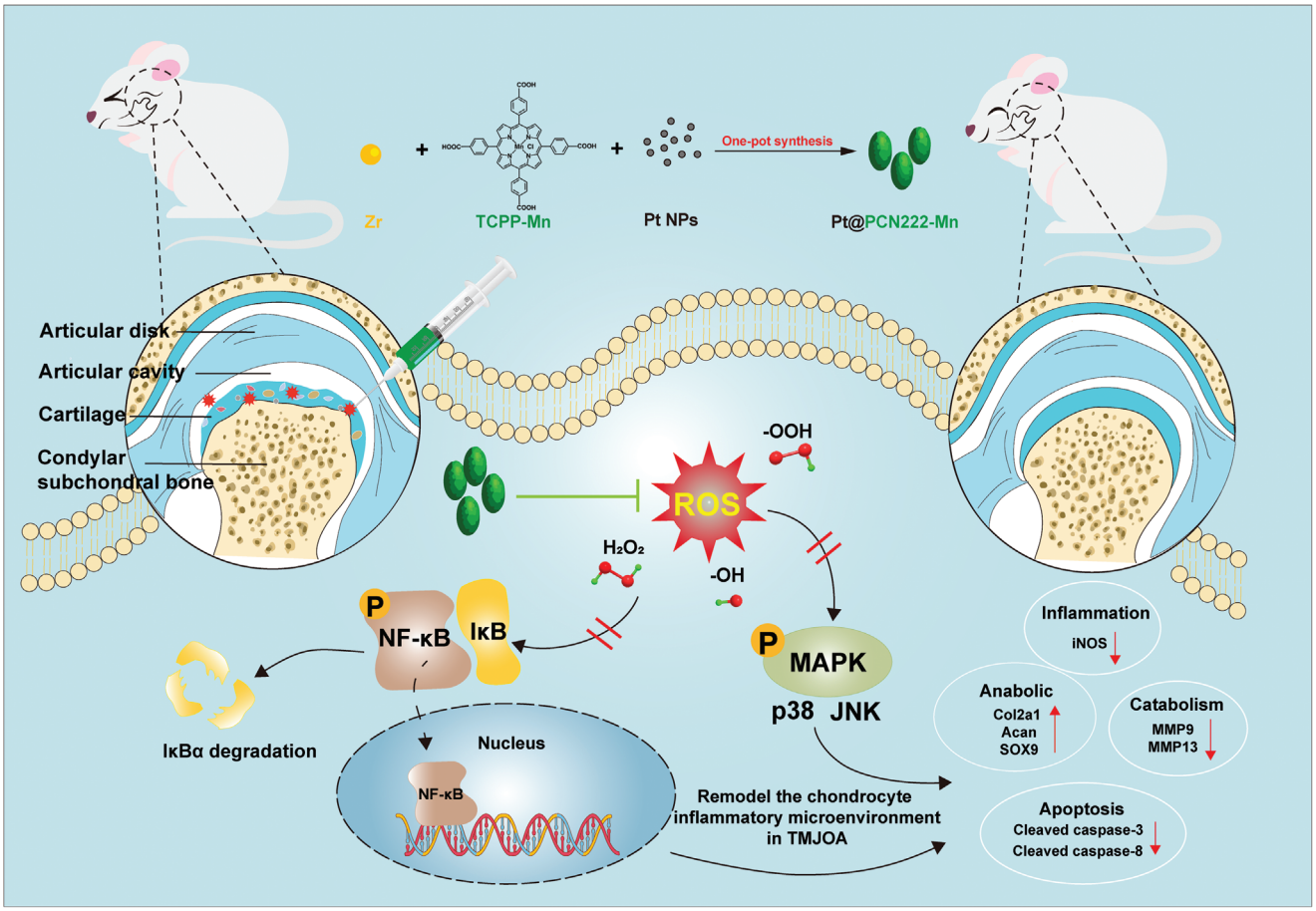

Scheme 1. Schematic illustration of the mechanism by which Pt@PCN222-Mn remodels the inflammatory microenvironment in TMJ OA. Pt@PCN222-Mn protects condylar chondrocytes by attenuating proinflammatory cytokines and mechanical injury-induced inflammation, reducing extracellular matrix catabolism, and preventing chondrocyte apoptosis through inhibition of ROS-NF-κB and MAPK signaling pathways. These protective effects suggest that Pt@PCN222-Mn shows therapeutic potential against TMJ OA.

modulates the chondrocyte inflammatory microenvironment by regulating inflammatory cytokine production, cartilage metabolism, and chondrocyte apoptosis.[8] Oxidative stress in TMJ OA induces redox-sensitive transcription factors such as nuclear factor kappa-B (NF-κB), triggering proinflammatory phenotypic alterations in TMJ OA tissue, including inducible nitric oxide synthase (iNOS), interleukin (IL)-6, and cyclooxygenase (COX)-2.[9] In conjunction with NF-κB, the mitogen-activated protein kinase (MAPK) signaling pathway modulates genes associated with cartilage catabolism and inflammation in response to oxidative stress.[10] Previous studies have found that Resveratrol, an antioxidant, may inhibit chondrocyte apoptosis in mouse TMJ OA through the COX-2/NF-κB pathway.[11] Therefore, we reason that inhibiting ROS overproduction and regulating oxidative stress may be an effective therapeutic approach for TMJ OA. Nanozymes are nanomaterials with enzyme-like activities.[12] They can compensate for the ease of denaturation and the high cost of natural enzymes.[13] In addition, nanozymes have the advantages of high specific surface activity, abundant designability, high biocompatibility, and large-scale production. Therefore, nanozymes have been widely used in biosensing, environmental protection, and disease therapy.[14] Recently, to alleviate oxidative stress in OA pathogenesis,[15] Sharma et al. synthesized polyethylene glycol (PEG)-MnO_2 nanoparticles that are capable of sustained retention in the joint space, targeted cartilage, and moderated oxidative stress in OA.[16] Cai et al. proposed a nanozyme therapeutic strategy using HPBzymes to remodel the chondrocyte microenvironment and delay OA both in vitro and in vivo.[17] In view of these successful results, clinical studies of nanomedicine with ROS-modulating functions on OA inflammation can be further explored. Pt@PCN222-Mn, a cascade nanozyme with multifunctional active sites, exhibits excellent ROS scavenging activity, excellent biocompatibility, and good water dispersibility. Encouragingly, Pt@PCN222-Mn has been demonstrated to reduce excess ROS in the treatment of inflammatory bowel disease.[18] Based on the excellent antioxidant therapeutic effect of Pt@PCN222-Mn, we hypothesized that Pt@PCN222-Mn may significantly lower excess ROS levels in the TMJ OA microenvironment, thus protecting chondrocytes and delaying TMJ OA. As shown in **Scheme 1**, our findings demonstrated that Pt@PCN222-Mn can protect chondrocytes, reduce inflammation, inhibit chondrocyte apoptosis, maintain ECM homeostasis, and provide therapeutic benefits in vivo. Furthermore, potential biological mechanism studies showed

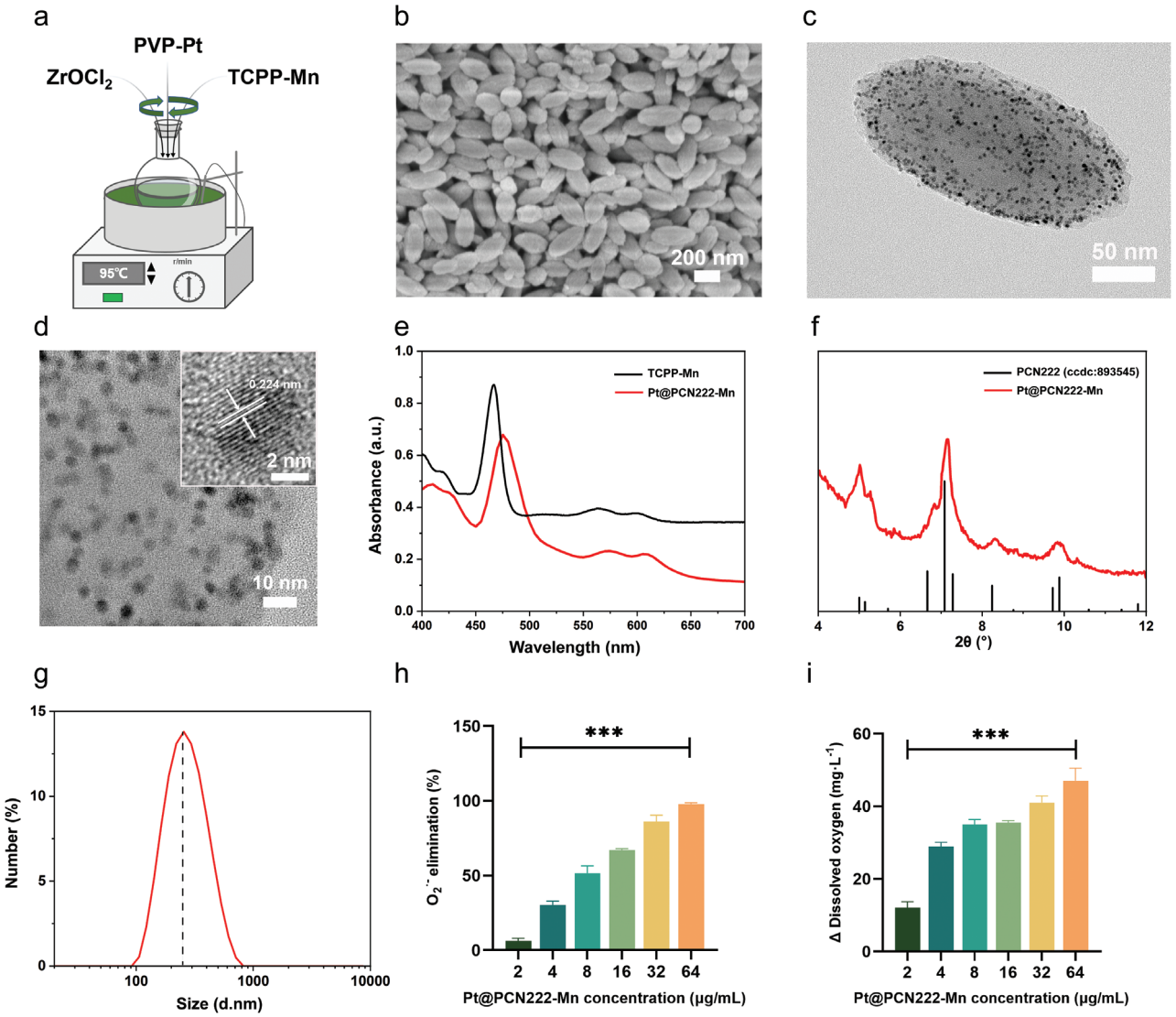

Figure 1. Characterization and enzyme-mimicking activity of Pt@PCN222-Mn. a) Synthetic scheme of Pt@PCN222-Mn. b) SEM image. c) TEM image and d) high-resolution TEM image. e) Absorption spectra of TCPP-Mn and Pt@PCN222-Mn. f) PXRD spectrum. g) DLS analysis. h) SOD-mimicking activity. i) CAT-mimicking activity of Pt@PCN222-Mn at different concentrations. *t*-test. Data are presented as mean ± SD ($n = 3$). $^{*}P < 0.05$, $^{**}P < 0.01$, $^{***}P < 0.001$. N.S., not significant. a.u., arbitrary units.

that Pt@PCN222-Mn remodels the TMJ OA inflammatory microenvironment by inhibiting the ROS-NF-κB and p38/MAPK signaling pathways. We believe this work sheds new light on the future clinical application of nanozymes in TMJ OA therapy and paves the way for new therapeutic avenues for chronic diseases associated with oxidative stress.

2. Results and Discussion

2.1. Synthesis, Characterizations, and Measurements of Enzyme-Mimicking Activities of Pt@PCN222-Mn

The synthesis of Pt@PCN222-Mn is shown in **Figure 1**a. Scanning electron microscope (SEM) and transmission electron microscope (TEM) imaging showed that the synthesized nanozyme was in the shape of a long spindle, uniformly dispersed, and ≈200 nm in size (Figure 1b,c). As shown in the high-resolution TEM image (Figure 1d), a lattice spacing of 0.224 nm could be observed, confirming the successful encapsulation of Pt NPs. The successful incorporation of tris(chlorisopropyl) phosphate (TCPP)-Mn was also confirmed by the UV–vis absorption spectrum in Figure 1e. The powder X-ray diffraction (PXRD) pattern showed that the nanozyme had three main diffraction peaks at 5.0°, 7.2°, and 9.9°, which is consistent with the results reported in the previous literature (Figure 1f).[40] Dynamic light scattering (DLS) revealed that the average hydrodynamic diameter of the nanozyme was ≈255 nm (Figure 1g). In addition, its zeta potential is ≈24.2 mV (Figure S1, Supporting Information). Thus, the successful synthesis of Pt@PCN222-Mn was confirmed. Then, we evaluated the superoxide dismutase (SOD)-mimicking activ-

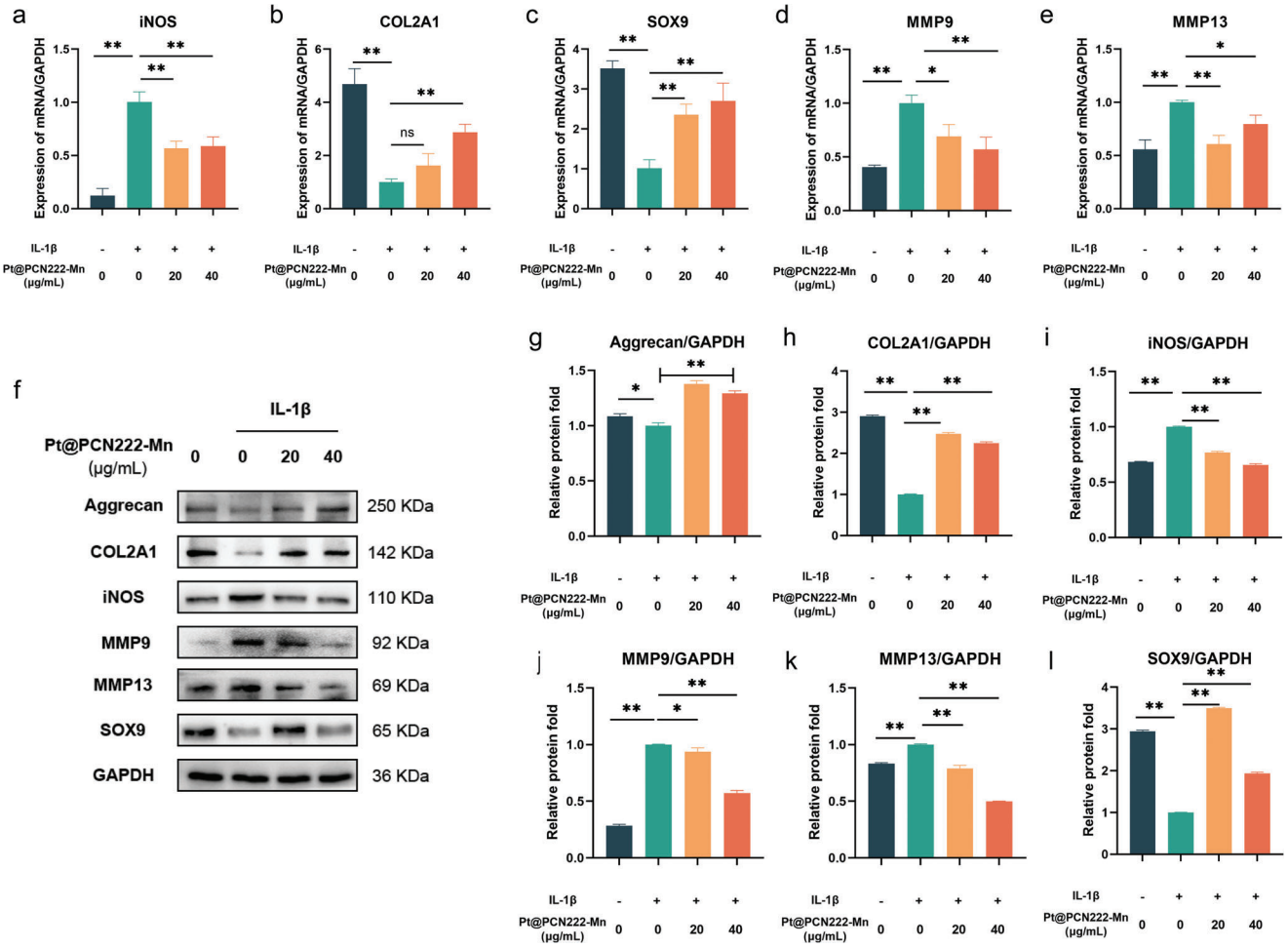

Figure 2. Pt@PCN222-Mn attenuates inflammation and inhibits ECM degradation in IL-1β-induced rat condylar chondrocytes. Relative mRNA expression of a) iNOS, b) COL2A1, c) SOX9, d) MMP9, and e) MMP13 stimulated with IL-1β and pretreated with Pt@PCN222-Mn in rat condylar chondrocytes. f–l) Effects of the key representative factors of inflammation and cartilage anabolism and catabolism protein levels after IL-1β induction as determined by Western blotting analyses. The Western Blot (WB) bands were cropped to clarify the lanes and the raw data are provided in Figure S6 in the Supporting Information. One-way ANOVA with Bonferroni test was performed. Data are presented as mean ± SD ($n = 3$). *$P < 0.05$, **$P < 0.01$, ***$P < 0.001$. N.S., not significant.

ity of Pt@PCN222-Mn by using an SOD detection kit, and the results revealed that the SOD-mimicking activity of Pt@PCN222-Mn was dose dependent. At a concentration of 36 μg mL^{-1}, the $O_2^{\bullet-}$ eliminating rate was close to 100% (Figure 1h). In addition, we monitored O_2 generation by the decomposition of H_2O_2 to evaluate the catalase (CAT)-mimicking activity of Pt@PCN222-Mn. As shown in Figure 1i, Pt@PCN222-Mn exhibits excellent CAT mimetic activity. Therefore, we concluded that Pt@PCN222-Mn has excellent SOD- and CAT-mimicking activities as well as good water dispersibility, which is consistent with previous studies.

2.2. Pt@PCN222-Mn Attenuates Inflammation and Inhibits ECM Degradation in Interleukin 1 Beta (IL-1β)-Induced Rat Condylar Chondrocytes

IL-1β is considered to be the major proinflammatory cytokine in TMJ OA, leading to increased matrix metalloproteinases and aggrecanases (ADAMTS). The synthesis of major ECM components, such as SOX9, collagen type II (Col2A1), and aggrecan (ACAN), is further inhibited, disrupting metabolic homeostasis in cartilage.[19] Therefore, IL-1β is commonly induced in vitro to mimic the TMJ OA inflammatory microenvironment.[20] First, we isolated and identified primary condylar chondrocytes from 2-week-old Wistar rats and then used IL-1β to induce rat condylar chondrocyte inflammation to explore the effect of Pt@PCN222-Mn on TMJ OA inflammation in vitro (Figure S2, Supporting Information). The cell counting kit (CCK)-8 method was used to evaluate the effect of different concentrations (0–200 μg mL^{-1}) of Pt@PCN222-Mn on the cytotoxicity of rat condylar chondrocytes (Figure S3, Supporting Information). The results showed that the cytotoxicity of 20 and 40 μg mL^{-1} Pt@PCN222-Mn was relatively small within 24 h, so we chose the two concentrations as the follow-up experimental objects. In chondrocytes, IL-1β stimulates the synthesis of cytokines such as iNOS, leading to aggravation of TMJ OA. Expression of iNOS in chondro-

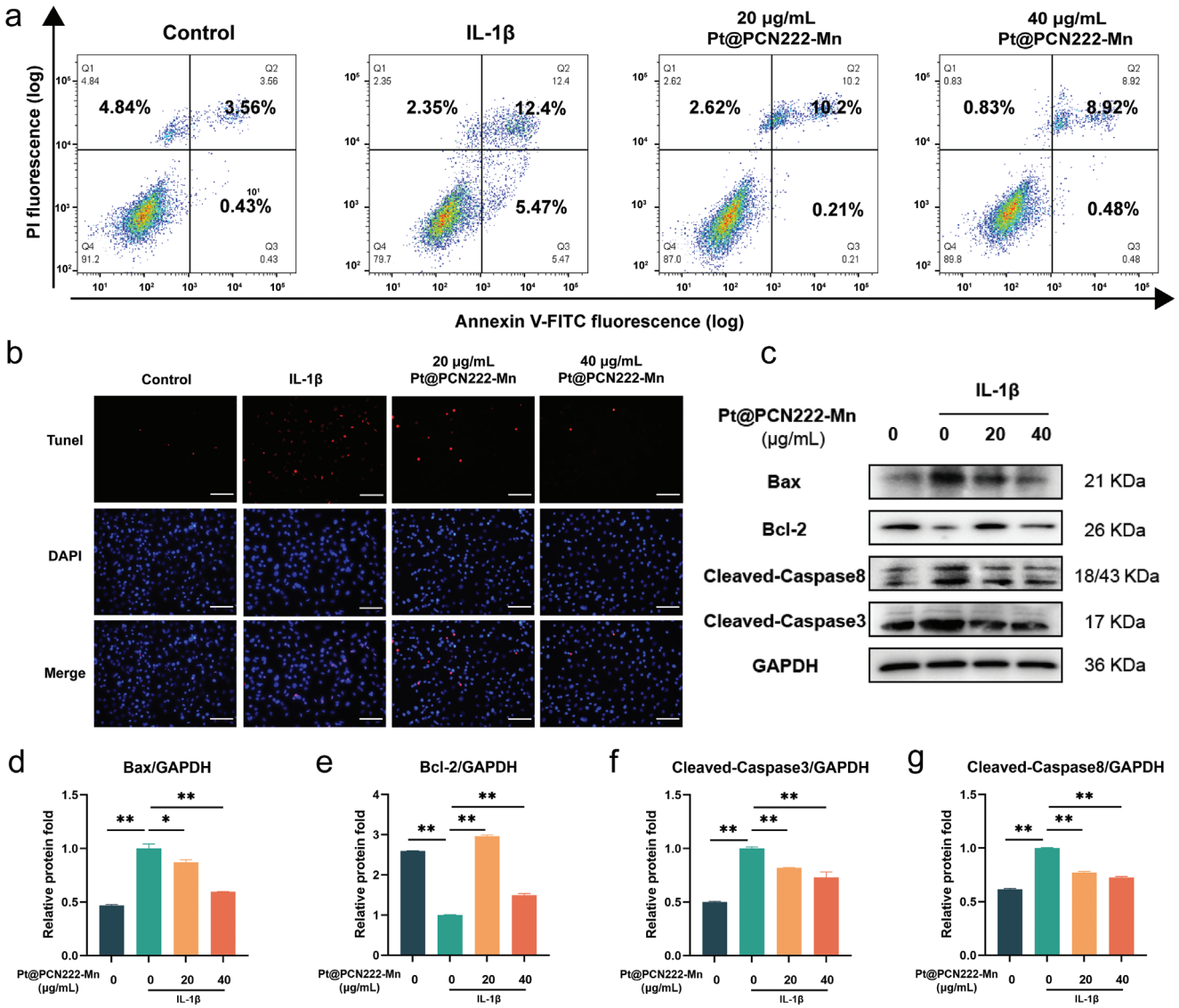

Figure 3. Pt@PCN222-Mn reduces apoptosis of inflammatory rat condylar chondrocytes. a) Effect of Pt@PCN222-Mn on chondrocyte apoptosis after IL-1β-induced treatment by flow cytometry. b) Pt@PCN222-Mn exerts an antiapoptosis effect in IL-1β-induced chondrocytes, as seen from the TUNEL assay. Scale bar: 100 μm. c–g) Effects of Pt@PCN222-Mn on the Bax, Bcl-2, Cleaved-Caspase3, and cleaved-Caspase8 protein levels after IL-1β induction as determined by Western blotting analyses. Protein levels were normalized to that of glyceraldehyde-3-phosphate dehydrogenase (GAPDH). The WB bands were cropped to clarify the lanes and the raw data are provided in Figure S7 in the Supporting Information. One-way ANOVA with Bonferroni test was performed. Data are presented as mean ± SD ($n = 3$). *$P < 0.05$, **$P < 0.01$, ***$P < 0.001$. N.S., not significant.

cytes to evaluate the anti-inflammatory effect of Pt@PCN222-Mn. **Figure 2**a shows that Pt@PCN222-Mn decreased iNOS messenger RNA (mRNA) levels in condylar chondrocytes, as determined by quantitative real time–polymerase chain reaction (qRT–PCR). Increased iNOS stimulates chondrocytes to synthesize NO. In turn, it upregulates matrix metalloproteinase activity and prevents the expression of ECM synthesis-related factors, resulting in chondrocyte damage. In Figure 2b–e, pretreatment with Pt@PCN222-Mn significantly downregulated the increase in MMP9 and MMP13 mRNA levels induced by IL-1β. At the same time, the mRNA expression of key genes in ECM synthesis, such as COL2A1 and SOX9, also increased significantly after Pt@PCN222-Mn treatment. In addition, Western Blot results showed that the levels of related proteins were consistent with their mRNA levels (Figure 2f–l). Taken together, Pt@PCN222-Mn can effectively reduce inflammatory cytokines and inhibit ECM degradation in the TMJ OA microenvironment.

2.3. Pt@PCN222-Mn Reduces Apoptosis of Inflammatory Rat Condylar Chondrocytes

When chondrocytes are stimulated by IL-1β, the resulting inflammatory response causes chondrocytes to rapidly age or undergo apoptosis.[21] To observe the antiapoptosis properties of Pt@PCN222-Mn, Annexin V-fluoresceinIsothiocyanate

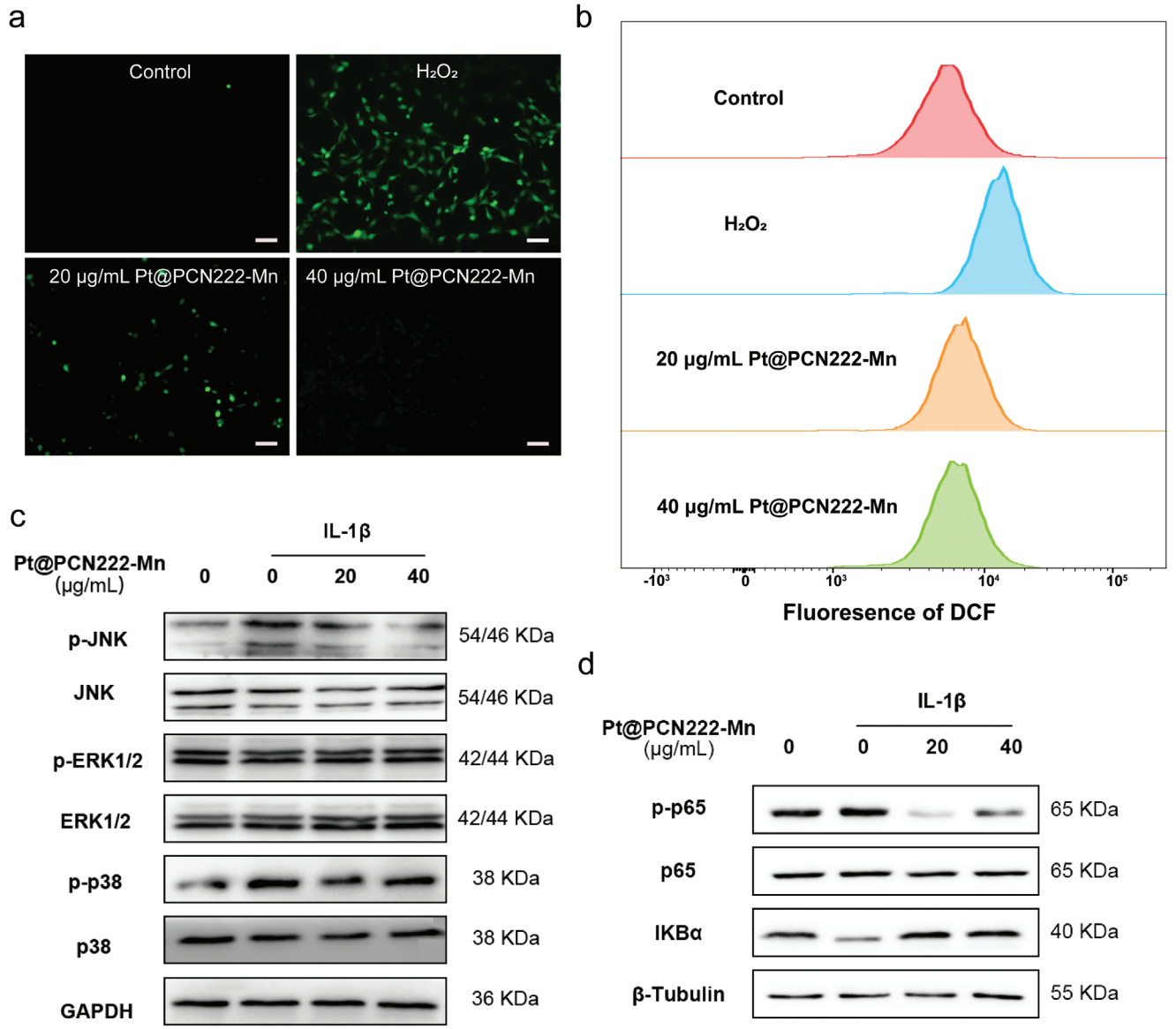

Figure 4. Pt@PCN222-Mn suppresses the ROS-NFκB and MAPK signaling pathways. a) Effect of Pt@PCN222-Mn on ROS levels after IL-1β treatment as stained by DCFH-DA and analyzed by fluorescence microscopy. Scale bar: 100 μm. b) Effect of Pt@PCN222-Mn on ROS levels after H_2O_2 treatment as determined by flow cytometry. c) Effect of Pt@PCN222-Mn on the protein expression of the key molecules of the MAPK signaling pathway and d) the inhibitory effect of Pt@PCN222-Mn on the NF-κB signaling pathway. The WB bands were cropped to clarify the lanes, and the raw data are provided in Figure S8 in the Supporting Information. One-way ANOVA with Bonferroni test was performed. Data are presented as mean ± SD ($n = 3$). $^*P < 0.05$, $^{**}P < 0.01$, $^{***}P < 0.001$. N.S., not significant.

(FITC)/PI staining measurement was used. As shown in **Figure 3**a, flow cytometry analysis showed that the percentage of late apoptosis or necrosis was significantly increased in the IL-1β-treated group compared with the control group, while the Pt@PCN222-Mn-treated group could significantly reduce this trend. Furthermore, TdT-mediated dUTP nick-end labeling (TUNEL) fluorescence staining was used to characterize DNA damage. As shown in Figure 3b, TUNEL-positive chondrocytes were significantly reduced after Pt@PCN222-Mn treatment, indicating that Pt@PCN222-Mn can protect chondrocytes to a certain extent from DNA damage. Several studies have shown that chondrocyte apoptosis occurs predominantly via the endogenous mitochondrial pathway and the exogenous death receptor pathway. Among them, Bax is a proapoptotic molecule in the endogenous pathway, and Bcl-2 is an antiapoptotic molecule. The exogenous pathway is activated by ligands of members of the tumor necrosis factor receptor superfamily, resulting in the activation and cleavage of cysteinyl aspartate-specific proteinase (Caspase)-3 and -8. As shown in Western Blot, Pt@PCN222-Mn effectively inhibited the production of proapoptotic molecules and Caspase-3 and -8 cleavage and expression in chondrocytes while enhancing antiapoptotic molecule expression (Figure 3c–g). These findings indicate that Pt@PCN222-Mn can effectively inhibit the apoptosis of inflammatory chondrocytes.

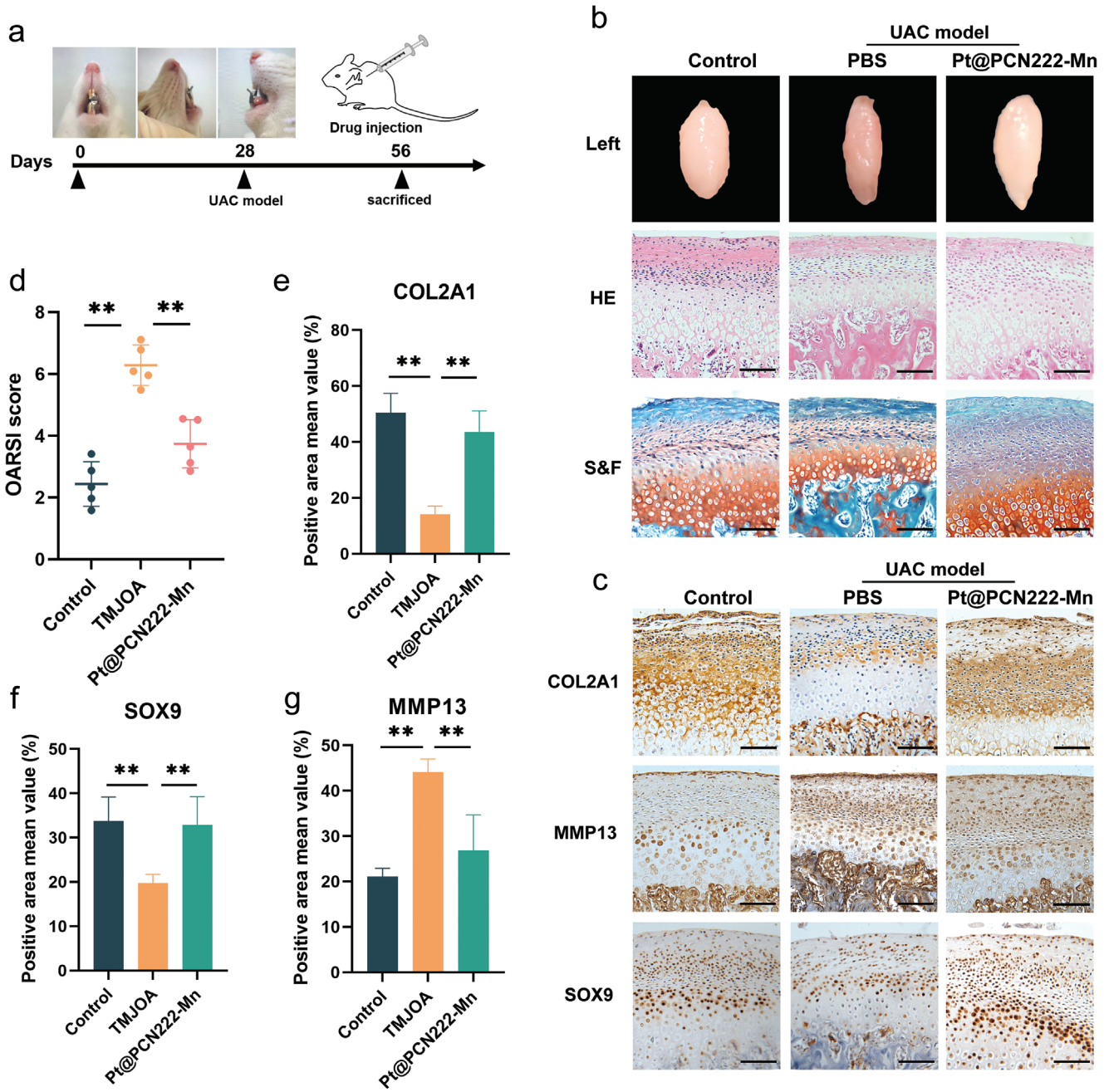

Figure 5. Pt@PCN222-Mn delays the progression of TMJOA in vivo. a) Schematic meditation diagram shows the UAC rats that received Pt@PCN222-Mn treatment and were euthanized at the 4-week posttreatment. b) Macroscopic appearance, HE, and Safranin-O/Fast Green staining of condyles from rats after treatment for 4 weeks. Scale bar: 100 μm. c) IHC staining of condyles from rats after treatment for 4 weeks. Scale bar: 100 μm. d) OARSI scores for histology of articular cartilage after treatment for 4 weeks. e–g) Quantification data for IHC positive area level in (c). One-way ANOVA with Bonferroni test was performed. Data are presented as mean ± SD ($n = 6$). $^{*}P < 0.05$, $^{**}P < 0.01$, $^{***}P < 0.001$. N.S., not significant. HE: hematoxylin-eosin, IHC: immunohistochemistry, OARSI: Osteoarthritis Research Society International.

2.4. Pt@PCN222-Mn Suppresses the ROS-NF-κB and MAPK Signaling Pathways

In chondrocytes, excessive production of ROS disrupts the defense function of the antioxidant system, which is one of the factors contributing to the pathogenesis of TMJ OA. During this process, ROS act as intermediate signaling molecules for various signaling factors, resulting in an upregulation of various inflammatory factors and cytokines, accelerating chondrocyte apoptosis, and degradation of the extracellular matrix. Studies have shown that ROS are overproduced in the chondrocyte inflammatory microenvironment.[22] Therefore, we used the H_2O_2-stimulated chondrocyte model to test the in vitro ROS scavenging ability of Pt@PCN222-Mn. ROS probe 2,7-dichlorodihydrofluorescein di-

acetate (DCFH-DA) fluorescence (**Figure 4**a) and flow cytometry analysis (Figure 4b) showed that treatment with Pt@PCN222-Mn significantly reduced the ROS scavenging ability. The pathogenesis of TMJ OA involves several inflammatory signaling pathways, including NF-κB, janus kinase (JAK)/signal transducer and activator of transcription (STAT), Wnt, and MAPK.[23] To assess the possible anti-inflammatory and antiapoptosis effects of Pt@PCN222-Mn, we detected several key proteins of the classical inflammatory pathways of NF-κB and MAPK. We observed that Pt@PCN222-Mn could inhibit the phosphorylation of c-Jun N-terminal kinase (JNK) protein and p38 protein but not extracellular regulated protein kinases (ERK) protein (Figure 4c and Figure S4, Supporting Information). The possible reason is that the signal transduction pathways involved in the MAPK subfamily perform different functions. The JNK and p38 signaling pathways are essential for stress responses such as inflammation and apoptosis, while ERK is primarily responsible for regulating differentiation and growth. Meanwhile, western blot analysis showed that IL-1β-induced increase in p65 protein phosphorylation was inhibited by Pt@PCN222-Mn, and the degradation of IκBα protein upon IL-1β stimulation was also rescued by Pt@PCN222-Mn treatment (Figure 4d). The reason may be that it inhibits the degradation of IκBα protein in the cytoplasm and the nuclear entry of NF-κB dimer under inflammatory conditions. Based on the above findings, we found that Pt@PCN222-Mn remodels the IL-1β-induced chondrocyte microenvironment by attenuating the ROS-NF-κB and MAPK signaling pathways.

2.5. Pt@PCN222-Mn Delayed TMJ OA In Vivo

To investigate the effect of Pt@PCN222-Mn on TMJ OA in vivo, a rat occlusal disorder model created by unilateral anterior crossbite (UAC) was established.[25] The experimental mode is shown in **Figure 5**a. The microscopic image of the control group showed that the articular cartilage was smooth and complete, and hydroethidine (HE) staining indicated that the cartilage layer was complete. Classical chondrocyte morphology can be observed in fibrocartilage, proliferative cartilage, prehypertrophic cartilage, and hypertrophic cartilage. Additionally, the safranin O-positive staining area was mainly concentrated in the hypertrophic layer. In the TMJ OA group, the microscopic image revealed an irregular surface that was prone to redness and thinness, and histological staining revealed a substantial reduction in the number of chondrocytes, disordered cartilage structure, irregular arrangement, and reduced safranin O-positive staining area and proteoglycan content. In the Pt@PCN222-Mn group, the inflammatory state of condylar tissue was significantly recovered, the cartilage arrangement was more orderly than that in the TMJ OA group, and the number of chondrocytes and the level of proteoglycans were increased (Figure 5b). Likewise, the osteoarthritis research society international (OARSI) score was significantly lower in the TMJ OA group than in the control group, while the score was improved after Pt@PCN222-Mn treatment (Figure 5d). In addition, immunohistochemistry (IHC) showed that Pt@PCN222-Mn treatment reversed the upregulation of MMP13 and the loss of the ECM synthesis-related molecules COL2A1 and SOX9 (Figure 5c,e–g). In addition, we evaluated splanchnic tissue sections from each group of rats and determined that there was no apparent biological toxicity of Pt@PCN222-Mn (Figure S5, Supporting Information). Overall, these results reveal an in vivo therapeutic effect of Pt@PCN222-Mn, which can inhibit ECM catabolism and slow TMJ OA progression.

3. Conclusion

In conclusion, we found that Pt@PCN222-Mn could mediate the ROS-NF-κB and MAPK signaling pathways in the inflammatory microenvironment of TMJ OA to remodel its functions, thereby exerting anti-inflammatory and antiapoptotic effects to protect cartilage. Pt@PCN222-Mn nanozyme could increase ECM synthesis and reduce matrix metalloproteinase expression to protect condylar cartilage and delay the TMJ OA therapeutically. This study not only provides a novel and effective strategy for the treatment of TMJ OA but also opens up a new application direction for the inflammatory therapeutic function of nanozymes.

4. Experimental Section

Reagents and Materials: Polyvinyl pyrrolidone (PVP) and HE were purchased from Aladdin (Shanghai, China). H_2PtCl_6 was supplied by Sigma-Aldrich (St. Louis, MO, USA). $ZrOCl_2{\cdot}8H_2O$ was provided by Energy Chemical (Shanghai, China). Collagenase II and chemiluminescent reagents were supplied by Biosharp (Anhui, China). Recombinant rat IL-1β was obtained from PeproTech (Rocky Hill, NJ, USA). Radio immunoprecipitation assay (RIPA) lysis buffer, phenylmethanesulfonyl fluoride (PMSF), 4% paraformaldehyde (PFA), and 4′,6-diamidino-2-phenylindole (DAPI) were purchased from Beyotime (Jiangsu, China). Dulbecco's modified Eagle medium (DMEM), phosphate buffered saline (PBS), and trypsin–ethylene diamine tetraacetic acid (EDTA) (0.25%) were obtained from Thermo Fisher Scientific (Waltham, MA, USA). Details of the assay kits used in this study were listed in Table S1 in the Supporting Information.

Instrumentation: SEM imaging was performed on a Zeiss Ultra 55 microscope. TEM images were collected on an FEI Tecnai F20 TEM. PXRD patterns were measured on a Rigaku Ultima diffractometer (Thermo Fisher Scientific, USA) using Cu K_α radiation. The UV–visible absorption spectra were obtained with a UV–visible spectrophotometer with a 1 cm quartz cell (Purkinje, China) and a microplate reader (SpectraMax M2e, China). DLS and zeta potentials were measured by using a Malvern Zetasizer Nano ZS90 at 25 °C in water. The generated oxygen was monitored by using a SevenExcellence dissolved oxygen meter. Quantitative real time (RT)–PCR was performed on an ABI-7300 real-time PCR system (Applied Biosystems, CA, USA). The Western blot membranes were visualized using a Tanon imaging system (Shanghai, China). Fluorescence images were obtained with a fluorescence microscope (Leica Microsystems, Germany). Rat condylar specimen images were collected by an optical microscope (Leica Microsystems, Germany).

Measurement of Enzyme-Mimicking Activity: An SOD assay kit was used to evaluate the SOD-mimicking activity of Pt@PCN222-Mn. The SOD-mimicking activity of different concentrations of Pt@PCN222-Mn can be colorimetrically monitored by using a microplate reader. To evaluate the CAT-mimicking activity of Pt@PCN222-Mn, different concentrations of Pt@PCN222-Mn and 5 mM H_2O_2 were sequentially added to 3 mL of water, and the Pt@PCN222-Mn was removed by centrifugation after incubation at room temperature for 30 min. The CAT-mimicking activity of Pt@PCN222-Mn was determined by detecting the dissolved oxygen (mg L^{-1}) content in the solutions by a dissolved oxygen detector. Accuracy was assessed by repeated analyses ($n = 3$).

Preparation and Characterization of Pt@PCN222-Mn: The synthetic methodology of Pt@PCN222-Mn was the same as before.[18] First, 266 mg PVP was dissolved in 90 mL methanol, and 10 mL H_2PtCl_6 was added, followed by 3 h of reflux at 75 °C, and PVP-Pt NPs were obtained by precipitation and purification. As a follow-up experiment, 20 mg TCPP-Mn, 60 mg $ZrOCl_2{\cdot}8H_2O$, and 580 mg benzoic acid were dissolved in 15 mL N,N-

dimethylformamide (DMF). The mixture was stirred (300 rpm) at 90 °C. Meanwhile, 5 mL of the as-synthesized PVP-Pt NPs solution was added dropwise to the mixture and stirred at 90 °C for another 5 h. The pellet was collected after cooling. The morphology and physical properties of Pt@PCN222-Mn were evaluated using a Quanta 200 SEM. The phase composition and crystallinity of the synthesized powders were determined using a Rigaku Ultima diffractometer. The particle size of Pt@PCN222-Mn was measured by a Malvern-Zetasizer Nano ZSP instrument.

Isolation and Culture of Rat Condylar Chondrocytes: Two-week-old Wistar rat TMJ condylar cartilage tissues were isolated under sterile conditions. Tissues were washed three times with sterile PBS, cut into pieces of ≈1–2 mm^3, and subsequently digested with 0.25% trypsin and 0.2% collagenase II. After terminating digestion, the chondrocytes were collected and resuspended in DMEM containing 20% fetal bovine serum (FBS) at 37 °C in a humidified atmosphere containing 5% CO_2. The medium was changed 48 h after primary cell seeding. The cells were used for the second passage (P2) in subsequent experiments. In vitro experiments were replicated three times using the same rat condylar chondrocytes in each replicate.

Cell Viability: Pt@PCN222-Mn was evaluated for its biocompatibility with chondrocytes by seeding chondrocytes at a density of 5×10^3 cells in 96-well plates. Subsequently, the medium was changed to contain different concentrations of Pt@PCN222-Mn after the cells had adhered. In accordance with the instructions, cell viability was determined using a microplate reader after 24 h with the CCK-8 cell viability kit.

Stimulation of Rat Condylar Chondrocytes: Condylar chondrocytes were seeded into six-well plates at a density of 2×10^5 per well. Chondrocytes were pretreated with 20 and 40 μg mL^{-1} Pt@PCN222-Mn for 2 h and then stimulated with IL-1β (10 ng mL^{-1}) for 24 h.

Quantitative Reverse Transcription PCR: Total RNA was isolated from treated chondrocytes using a FastPure Cell/Tissue Total RNA Isolation Mini Kit according to the manufacturer's instructions and then transcribed into complementary DNA (cDNA) using a HiScript III 1st Strand cDNA Synthesis Kit. RNA quality was determined by measuring the optical density at the ratio of 260 and 280 nm. The primers used are listed in Table S2 in the Supporting Information.

Western Blotting Analyses: The treated chondrocytes were washed three times with PBS and then lysed in RIPA buffer supplemented with PMSF on ice to extract total cellular protein. A bicinchoninic acid (BCA) protein kit was used to determine the total protein concentration. Protein samples were loaded and separated by 10% to 15% dodium dodecyl sulfate–polyacrylamide gelelectrophoresis (SDS–PAGE) electrophoresis and transferred to polyvinylidene difluoride (PVDF) membranes, which were blocked with 5% nonfat milk for 1 h at room temperature and then incubated with specific primary antibodies overnight at 4 °C. The related secondary antibody (1:8000) was then incubated at room temperature for 2 h after washing with TBST. Finally, the membrane was visualized with a chemiluminescent reagent. Primary antibody dilutions for western blot analysis are listed in Table S3 in the Supporting Information.

Flow Cytometry for Detection of Apoptosis: Treated chondrocytes were harvested with EDTA-free trypsin, centrifuged, and washed with PBS three times. The apoptosis rate of chondrocytes was detected using the Annexin V-FITC/PI apoptosis kit according to the manufacturer's instructions and all samples were analyzed by using a board of flow cytometer (BD FACS) flow cytometer.

TUNEL Method: The TUNEL assay was used to evaluate the antiapoptosis ability of Pt@PCN222-Mn. The treated chondrocytes were fixed with 4% PFA for 30 min and then perforated with 0.2% Triton X-100 for 30 min. After washing three times, the chondrocytes were stained by using an in situ cell death detection kit and DAPI according to the manufacturer's instructions. Imaging was performed using a fluorescence microscope and quantified by ImageJ software.

Assay of ROS Scavenging Ability In Vitro: The in vitro ROS scavenging ability of Pt@PCN222-Mn was determined by using an ROS assay kit. First, chondrocytes were seeded on a 12-well plate at a density of 1×10^5 cells per well and incubated overnight. Then, the chondrocytes were pretreated with 20 and 40 μg mL^{-1} Pt@PCN222-Mn for 2 h, stimulated with 100 μM H_2O_2 for 4 h, and incubated with 5 μM DCFH-DA at 37 °C for 30 min in the dark. The results were measured by using a fluorescence microscope and a BD FACS flow cytometer.

Establishment of TMJ OA Model and Animal Experiment: Animals were acquired from Beijing Wetahe Laboratory Animal Technology Co., Ltd. (Beijing, China). The animal experiment was approved by the Ethics Committee of Nanjing Medical University, and the rat housing and welfare procedures were in accordance with the guidelines of the Institutional Animal Care and Use Committee (IACUC-2111005). A total of 18 male Wistar rats (4-week-old) were randomly divided into three groups (six rats in each group) as follows: control group (sham-induced TMJ OA plus PBS injection); UAC group (occlusion-induced TMJ OA plus PBS injection), and Pt@PCN222-Mn group (occlusion-induced TMJ OA plus Pt@PCN222-Mn injection). Following the previous approach,[24] an occlusal disturbance was experimentally generated by UAC in the UAC group and Pt@PCN222-Mn group. Rats were anesthetized intraperitoneally with 0.1% sodium pentobarbital (per 100 g body weight), and then a pair of specially made metal crowns were bonded to the left maxillary and mandibular incisors of rats to induce occlusal disturbance. Make sure the metal crown is kept at least once a day. Meanwhile, in the control group, rats were subjected to a similar procedure for sham induction. After 4 weeks, the rat UAC model was established. Bilateral TMJ injections were performed in the UAC group and the Pt@PCN222-Mn group under anesthesia. The injection method was first to touch the back of the zygomatic arch, then advance the needle forward, touch the top of the articular fossa, and then 30 μL Pt@PCN222-Mn (40 μg mL^{-1}) or PBS was slowly injected, repeated twice a week, and the rats were sacrificed 4 weeks after the injection. The left TMJ condyle was used for histological analysis.

Histological Staining and OARSI Scoring System: HE staining was used to observe the condylar histochemical changes. Safranin O/Fast Green staining was performed to assess proteoglycan changes in the condylar tissues. First, condylar specimens were collected and fixed for 24 h in 4% PFA. The tissues were then decalcified in 10% EDTA for 4 weeks. Finally, after serial dehydration and paraffin embedding, serial sections were cut at a thickness of 4.5 μm parallel to the sagittal plane. Each section was stained with HE and Safranin O/Fast green in compliance with the manufacturer's protocol. The modified osteoarthritis research society international (OARSI) scoring system[25] was used to measure cartilage destruction in the condylar cartilage by three observers blinded to the experimental information.

Immunohistochemistry: Following deparaffinization, rehydration, and washing, the sections were subjected to antigen retrieval with boiling sodium citrate solution and quenched with 3% hydrogen peroxide. After blocking with 1% goat serum at 37 °C for 30 min, the sections were incubated at 4 °C with the following primary antibodies: anti-COL2A1 (1:100, Proteintech), anti-SOX9 (1:100, Cell Signaling Technology), and anti-MMP13 (1:100, Proteintech) and then with horseradish peroxidase (HRP)-conjugated secondary antibody for 1 h at 37 °C. An HRP-polymer antimouse/rabbit IHC kit (MXB, China) was used for observation. After hematoxylin counterstaining, differentiation, and dehydration in 1% alcohol, the sections were covered with neutral glue.[26] Images were visualized under an optical microscope. Positively stained cells were counted and percentages were calculated by ImageJ Pro Plus.

Statistical Analyses: Experiments were conducted in triplicate in this study. All results were analyzed using Student's *t*-test or one-way ANOVA with Bonferroni test with GraphPad Prism 9.0 software and data are expressed as mean ± SD. $P < 0.05$ was considered statistically significant.

Supporting Information

Supporting Information is available from the Wiley Online Library or from the author.

Acknowledgements

Z.Z., L.Y., and Y.L. contributed equally to this work. This work was supported by the National Natural Science Foundation of China (82170911),

Key Research Program in Jiangsu Province-Social Development Project (BE2021724), and a project funded by the Priority Academic Program Development of Jiangsu Higher Education Institutions (PAPD, 2018-87). After initial online publication, Figure 2f was replaced on April 17, 2023. In the original version, the raw Western Blot band of MMP9, provided in Figure S6, was missing. This correction does not affect the results and conclusions of this work.

Conflict of Interest

The authors declare no conflict of interest.

Data Availability Statement

The data that support the findings of this study are available from the corresponding author upon reasonable request.

Keywords

anti-inflammation, nanozymes, reactive oxygen species, temporomandibular joint osteoarthritis

Received: December 8, 2022
Revised: January 31, 2023
Published online: February 20, 2023

[1] a) P. Chantaracherd, M. T. John, J. S. Hodges, E. L. Schiffman, *J. Dent. Res.* **2015**, *94*, 79S; b) F. Liu, A. Steinkeler, *Dent. Clin. North. Am.* **2013**, *57*, 465.
[2] a) X. D. Wang, J. N. Zhang, Y. H. Gan, Y. H. Zhou, *J. Dent. Res.* **2015**, *94*, 666; b) B. Li, G. Guan, L. Mei, K. Jiao, H. Li, *J. Cell. Mol. Med.* **2021**, *25*, 4902.
[3] V. Machon, D. Hirjak, J. Lukas, *J. Cranio-Maxillofac. Surg.* **2011**, *39*, 127.
[4] a) A. M. Abouelhuda, A. K. khalifa, Y.-K. Kim, S. A. Hegazy, *J. Korean Assoc. Oral Maxillofac. Surg.* **2018**, *44*, 43; b) K. S. Lee, H. J. Kwak, J. M. Oh, N. Jha, Y. J. Kim, W. Kim, U. B. Baik, J. J. Ryu, *J. Dent. Res.* **2020**, *99*, 1363.
[5] J. P. McCain, R. H. Hossameldin, *Atlas Oral Maxillofac. Surg. Clin. N. Am.* **2011**, *19*, 145.
[6] a) F. Ou, Y. Huang, J. Sun, K. Su, Y. He, R. Zeng, D. Tang, G. Liao, *Inflammation* **2021**, *44*, 80; b) B. Hua, J. Qiu, X. Ye, X. Liu, *Bone* **2022**, *158*, 116372; c) H. Li, H. Guo, C. Lei, L. Liu, L. Xu, Y. Feng, J. Ke, W. Fang, H. Song, C. Xu, C. Yu, X. Long, *Adv. Mater.* **2019**, *31*, 1904535; d) X. Xu, B. Sui, X. Liu, J. Sun, *Bioact. Mater.* **2022**, https://doi.org/10.1016/j.bioactmat.2022.07.006
[7] P. Lepetsos, A. G. Papavassiliou, *Biochim. Biophys. Acta, Mol. Basis Dis.* **2016**, *1862*, 576.
[8] D. R. Park, J. Kim, G. M. Kim, H. Lee, M. Kim, D. Hwang, H. Lee, H.-S. Kim, W. Kim, M. C. Park, H. Shim, S. Y. Lee, *Nat. Commun.* **2020**, *11*, 4343.
[9] a) P. Luo, C. Feng, C. Jiang, X. Ren, L. Gou, P. Ji, J. Xu, *Cell Proliferation* **2019**, *52*, e12556; b) Y. Yamamoto, R. B. Gaynor, *Trends Biochem. Sci.* **2004**, *29*, 72; c) N. Ahmad, M. Y. Ansari, T. M. Haqqi, *J. Cell. Physiol.* **2020**, *235*, 6366.
[10] a) S. Rezatabar, A. Karimian, V. Rameshknia, H. Parsian, M. Majidinia, T. Azramezani Kopi, A. Bishayee, A. Sadeghinia, M. Yousefi, M. Monirialamdari, B. Yousefi, *J. Cell. Physiol.* **2019**, *234*, 14951; b) V. Ulivi, P. Giannoni, C. Gentili, R. Cancedda, F. Descalzi, *J. Cell. Biochem.* **2008**, *104*, 1393; c) Q. Shen, Y. Xiao, B. Cheng, Z. Sun, Y. Hu, H. Yang, Y. Luo, *Int. J. Biochem. Cell Biol.* **2021**, *141*, 106112.
[11] M. A. Panaro, V. Carofiglio, A. Acquafredda, P. Cavallo, A. Cianciulli, *Br. J. Nutr.* **2012**, *108*, 1623.
[12] a) L. Gao, J. Zhuang, L. Nie, J. Zhang, Y. Zhang, N. Gu, T. Wang, J. Feng, D. Yang, S. Perrett, X. Yan, *Nat. Nanotechnol.* **2007**, *2*, 577; b) H. Wei, L. Gao, K. Fan, J. Liu, J. He, X. Qu, S. Dong, E. Wang, X. Yan, *Nano Today* **2021**, *40*, 101269.
[13] a) J. Wu, X. Wang, Q. Wang, Z. Lou, S. Li, Y. Zhu, L. Qin, H. Wei, *Chem. Soc. Rev.* **2019**, *48*, 1004; b) Y. Huang, J. Ren, X. Qu, *Chem. Rev.* **2019**, *119*, 4357.
[14] a) Z. Chen, J.-J. Yin, Y.-T. Zhou, Y. Zhang, L. Song, M. Song, S. Hu, N. Gu, *ACS Nano* **2012**, *6*, 4001; b) L. L. Dugan, D. M. Turetsky, C. Du, D. Lobner, M. Wheeler, C. R. Almli, C. K.-F. Shen, T.-Y. Luh, D. W. Choi, T.-S. Lin, *Proc. Natl. Acad. Sci. USA* **1997**, *94*, 9434; c) Y. Guo, L. Deng, J. Li, S. Guo, E. Wang, S. Dong, *ACS Nano* **2011**, *5*, 1282; d) M. Huo, L. Wang, Y. Chen, J. Shi, *Nat. Commun.* **2017**, *8*, 357; e) B. Liu, Z. Sun, P.-J. J. Huang, J. Liu, *J. Am. Chem. Soc.* **2015**, *137*, 1290; f) F. Natalio, R. André, A. F. Hartog, B. Stoll, K. P. Jochum, R. Wever, W. Tremel, *Nat. Nanotechnol.* **2012**, *7*, 530; g) R. W. Tarnuzzer, J. Colon, S. Patil, S. Seal, *Nano Lett.* **2005**, *5*, 2573; h) N. Singh, M. A. Savanur, S. Srivastava, P. D'Silva, G. Mugesh, *Angew. Chem., Int. Ed.* **2017**, *129*, 14455; i) R. Zhang, B. Xue, Y. Tao, H. Zhao, Z. Zhang, X. Wang, X. Zhou, B. Jiang, Z. Yang, X. Yan, K. Fan, *Adv. Mater.* **2022**, *34*, 2205324; j) Z. Zhang, K. Fan, *Nanoscale* **2023**, *15*, 41; k) W. Zhen, Y. Liu, W. Wang, M. Zhang, W. Hu, X. Jia, C. Wang, X. Jiang, *Angew. Chem., Int. Ed.* **2020**, *132*, 9578.
[15] A. Lin, S. Liu, H. Wei, *Particuology* **2023**, *76*, 32.
[16] S. Kumar, I. M. Adjei, S. B. Brown, O. Liseth, B. Sharma, *Biomaterials* **2019**, *224*, 119467.
[17] W. Hou, C. Ye, M. Chen, W. Gao, X. Xie, J. Wu, K. Zhang, W. Zhang, Y. Zheng, X. Cai, *Bioact. Mater.* **2021**, *6*, 2439.
[18] Y. Liu, Y. Cheng, H. Zhang, M. Zhou, Y. Yu, S. Lin, B. Jiang, X. Zhao, L. Miao, C.-W. Wei, Q. Liu, Y.-W. Lin, Y. Du, C. J. Butch, H. Wei, *Sci. Adv.* **2020**, *6*, eabb2695.
[19] a) M. Kapoor, J. Martel-Pelletier, D. Lajeunesse, J.-P. Pelletier, H. Fahmi, *Nat. Rev. Rheumatol.* **2011**, *7*, 33; b) C. J. Malemud, *Curr. Opin. Rheumatol.* **2015**, *27*, 289.
[20] X. Liu, X. Li, B. Hua, X. Yang, J. Zheng, S. Liu, *Bone* **2021**, *143*, 115793.
[21] J. Xu, Y. Pei, J. Lu, X. Liang, Y. Li, J. Wang, Y. Zhang, *Int. Immunopharmacol.* **2021**, *90*, 107150.
[22] a) P. Lepetsos, K. A. Papavassiliou, A. G. Papavassiliou, *Free Radic. Biol. Med.* **2019**, *132*, 90; b) K. Lu, F. Ma, D. Yi, H. Yu, L. Tong, D. Chen, *J. Orthop. Transl.* **2022**, *32*, 21.
[23] M. Y. Ansari, N. Ahmad, T. M. Haqqi, *Biomed. Pharmacother.* **2020**, *129*, 110452.
[24] Y.-D. Liu, L.-F. Liao, H.-Y. Zhang, L. Lu, K. Jiao, M. Zhang, J. Zhang, J.-J. He, Y.-P. Wu, D. Chen, M.-Q. Wang, *Osteoarthritis Cartilage* **2014**, *22*, 302.
[25] H. Zhu, Y. Hu, C. Wang, X. Zhang, D. He, *Cell Death Dis.* **2020**, *11*, 284.
[26] L. Yuan, N. Zhao, J. Wang, Y. Liu, L. Meng, S. Guo, E. A. C. Wiemer, Q. Chen, Y. Mao, J. Ben, J. Ma, *Theranostics* **2021**, *11*, 7247.